



**Lattice distortion of oxygen monolayer on Ag(111) observed by scanning probe microscopy**Mitsuo Kimura  and Yoshiaki Sugimoto <sup>\*</sup>*Department of Advanced Materials Science, University of Tokyo, 5-1-5 Kashiwanoha, Kashiwa, Chiba 277-8561, Japan*

(Received 20 July 2022; revised 12 September 2022; accepted 12 September 2022; published 22 September 2022)

Oxygen molecules ( $O_2$ ) physically adsorbed on solid surfaces are of interest as low-dimensional spin systems. Monolayers of  $O_2$  adsorbed on an Ag(111) surface at a low density of less than 1 ML are observed at 4.5 K using scanning tunneling microscopy combined with atomic force microscopy with  $O_2$  terminated tips. Various domains with their specific density are mixed, each with different rotation angles to the substrate. The shape of the  $O_2$  lattice correlates with the rotation angle between the monolayer and the substrate. The domains with a rotation angle of greater than  $1.4^\circ$  can be explained by the model of on-line coincidence, which had previously been confirmed only for organic molecules. The coincidence with the substrate naturally explains the observed lattice distortion quantitatively. On the other hand, in domains at the rotation angle near  $0^\circ$ , the lattice distortion is smaller than that of previous study that attributed it to spin. Nevertheless, the length of the shortest distance between two  $O_2$  implies antiferromagnetic order.

DOI: [10.1103/PhysRevB.106.115432](https://doi.org/10.1103/PhysRevB.106.115432)**I. INTRODUCTION**

The oxygen molecule ( $O_2$ ) has two electrons in the outermost  $\pi^*$  molecular orbital, resulting in spin 1 [1]. The crystal structure of solid oxygen is determined by van der Waals, quadrupole, and exchange interactions. Since spin ordering affects the crystal structure, solid oxygen is called a spin-controlled crystal [2]. The  $\beta$  phase, which is present below ambient pressure, has an equilateral triangular lattice in the  $a$ - $b$  plane and a geometric frustration of spins. Below 24 K, the  $\beta$  phase undergoes a phase transition to the antiferromagnetically ordered  $\alpha$  phase, distorting the equilateral triangular lattice into an isosceles triangle.

Low-dimensional spin systems formed by the adsorption of  $O_2$  on the substrate have also attracted interest [3–10]. The Haldane state [11] has been identified in one-dimensional (1D) systems with  $O_2$  aligned within carbon nanotubes [3]. On the other hand, monolayers physically adsorbed on graphite, boron nitride, and Ag substrates have been studied as two-dimensional (2D) systems [4–10]. Experiments on the ortho-para conversion of molecular hydrogen showed that  $O_2$  physisorbed on Ag(111) retain their spin [12,13]. The magnetic structure of the  $O_2$  monolayer has also been discussed in structural analysis using low-energy electron diffraction (LEED) at 21 K [4]. In a low-density phase formed by adsorption of  $O_2$  with the molecular axis parallel to the surface, LEED spots in an almost isosceles triangular arrangement were observed. The LEED spot broadening showed that the lattice is distorted from an isosceles triangle. They interpreted this as the existence of antiferromagnetic domains that are mirror symmetric with each other. Real-space observations of the low-density phase on Ag(111) by scanning tunneling microscopy (STM) at 4.7 K confirmed the presence of

lattice distortions in the  $O_2$  monolayer [5]. From Monte Carlo calculations, the lattice distortion was interpreted as being caused by spin: the base that has the shortest intermolecular distance in the triangle lattice is antiferromagnetic, so one long side with ferromagnetic is longer than the other with antiferromagnetic. On the other hand, in  $O_2$  monolayers on graphite substrates, lattice distortions induced by the interaction between the monolayer and the substrate have been discussed [6]. Lattice distortion induced by the substrate has not been studied on Ag(111) substrates, although it could be misinterpreted as spin-induced lattice distortions.

In this study,  $O_2$  monolayers on Ag(111) were observed by atomic force microscopy (AFM) combined with STM to precisely quantify the lattice distortion and rotation angle with the substrate. High-resolution observation of various domains was performed at 4.5 K by AFM/STM using  $O_2$  terminated tips. Clear moiré patterns were observed, and the lattice geometry and the rotation angle were precisely determined for each domain.

**II. EXPERIMENT**

Experiments were performed at 4.5 K using a custom-built scanning probe microscope operating in an ultra-high vacuum. This microscope is a combined AFM and STM system using a quartz length-extension resonator as a force sensor and is capable of applying high magnetic fields up to 11 T perpendicular to the surface [14]. Experiments have been performed with magnetic fields ranging from 0 to 11 T. No changes due to the magnetic field were observed (see Supplemental Material [15]). The resolution was improved by attaching  $O_2$  to the tip apex. The Ag(111) surface was cleaned by Ar ion sputtering and annealing at 400 °C. The Ag(111) substrate was then placed in the microscope unit and cooled to 4.5 K. After adsorption of  $O_2$ , the sample was annealed to about 15–20 K below the desorption temperature of  $O_2$ ,

<sup>\*</sup>ysugimoto@k.u-tokyo.ac.jp

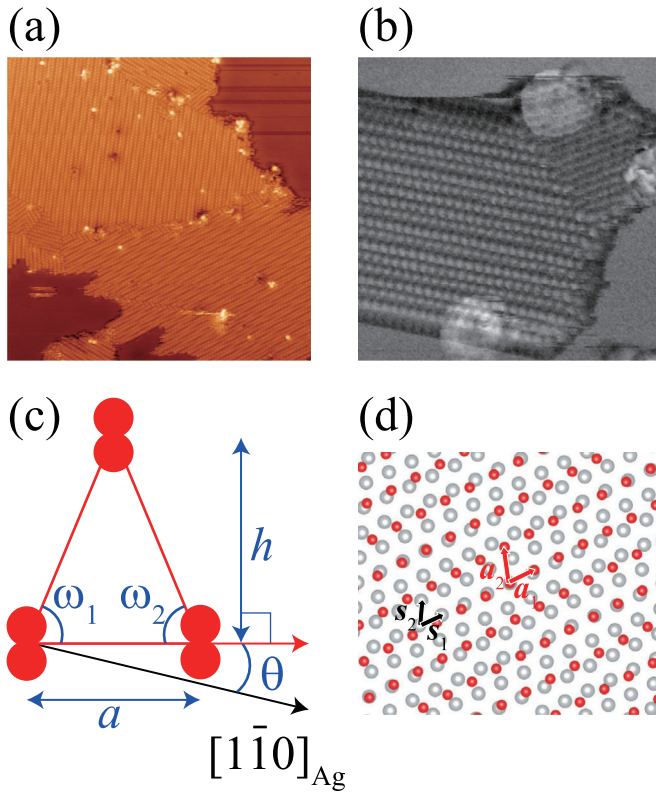


FIG. 1. (a) STM topographic image of monolayer of O<sub>2</sub> adsorbed on Ag(111) surface. The upper right area and lower bottom area are the Ag substrate.  $30 \times 30 \text{ nm}^2$ , sample bias  $V = 200 \text{ mV}$ , tunneling current  $I = 3 \text{ pA}$ , magnetic field  $B = 0 \text{ T}$ . (b) Constant height AFM image of O<sub>2</sub> monolayer.  $10 \times 10 \text{ nm}^2$ , resonance frequency  $f_0 = 988 \text{ kHz}$ , effective stiffness  $2k = 1.3 \text{ MN/m}$ ,  $B = 0.5 \text{ T}$ , color-map white:  $-0.7 \text{ Hz}$ , black:  $-1.5 \text{ Hz}$ . (c) Schematic view of a half unit cell of O<sub>2</sub> lattice. (d) Schematic model of O<sub>2</sub> lattice and Ag lattice obtained by FFT analysis of STM image corresponding to the lower area of (a).

and then cooled again to 4.5 K to start the experiment. The amount of adsorption was adjusted to produce a low-density phase formed at less than 1 ML. The obtained images were analyzed using GWYDDION software, including 2D fast Fourier transform (FFT) [16]. The model figure is fabricated using VESTA software [17].

### III. AFM/STM OBSERVATIONS

Figure 1(a) shows a STM image of a wide area that includes regions of Ag substrate and O<sub>2</sub> monolayer with a low-density phase. As in the previous study [5], individual O<sub>2</sub> are observed, and an isosceles triangular-like lattice can be seen. A schematic diagram of O<sub>2</sub> adsorbed on the substrate with the molecular axis parallel to the surface is shown in Fig. 1(c). Domain boundaries were observed, with one domain size averaging about a few-100 nm<sup>2</sup>. A feature not described in the previous study [5] was the observation of superstructures in each domain. These patterns of superstructures are considered to be moiré formed by the interaction with the substrate. The superstructure patterns are different for each domain, and the rotation angle with the substrate is considered

to be different for each domain. As will be shown later, this moiré pattern allows precise analysis of the lattice shape and rotation angle with the substrate.

Figure 1(b) shows an AFM image obtained at a constant height scan. Using the molecular functionalized tip, high-resolution images of the chemical structure of organic molecules [18,19] and the hydrogen bonding network structure of water molecules [20,21] can be obtained. In this study, individual O<sub>2</sub> were also observed by repulsive force with the tip. The superstructure of the O<sub>2</sub> monolayer was also observed by AFM. The origin of the moiré pattern is the physical corrugation of oxygen atoms caused by molecular orientation.

### IV. LATTICE SHAPE ANALYSIS

To precisely investigate the O<sub>2</sub> lattice, each domain was analyzed with a FFT. Figure 2 shows the results for 3 of 39 different domains. Figures 2(a), 2(c), and 2(e) are the STM images, and Figs. 2(b), 2(d), and 2(f) are the corresponding FFT images. In addition to spots corresponding to the O<sub>2</sub> lattice, spots of the superstructure are observed. As shown in Fig. 2(d), the spots of the O<sub>2</sub> lattice are indicated by arrows, and the spots of the superstructure are surrounded by an ellipse. The spot of the superstructure is known to be pointed by the vector of the difference between the reciprocal lattice vector of the adsorption layer and that of the substrate [22]. This property provides information on the lattice of the Ag substrate that is not directly observed by STM. We used the resulting triangular lattice of Ag substrates (lattice constant  $d = 2.89 \text{ \AA}$ ) to correct the FFT image by an affine transform to remove the effect of image distortion due to scanning. This allowed precise measurement of the O<sub>2</sub> lattice and their rotational angles with the substrate. By fitting the spots in the FFT image with a 2D Gaussian function, the shape of the triangular lattice can be analyzed. Table I summarizes the lattice shapes of the O<sub>2</sub> monolayer and their rotation angles with the substrate for each domain in Fig. 1 and Fig. 2, together with data from previous studies. The length of the base  $a$ , the length of the perpendicular  $h$ , the base angles  $\omega_1$  and  $\omega_2$ , and the rotation angle with the substrate  $\theta$  are defined in the schematic diagram shown in Fig. 1(c). We defined  $\theta = 0$  when the direction in which the O<sub>2</sub> are most closely aligned is the same as the crystallographic direction of the Ag surface,  $[1\bar{1}0]$ . We obtained  $\theta \approx 0$  in Fig. 2(a) as reported in a previous study by STM [5]. In addition, the domains with  $\theta \neq 0$  were identified in real space as Figs. 2(c) and 2(e). The existence of such domains had been pointed out in a previous study by LEED [4].

### V. LATTICE SHAPE VS ROTATION ANGLE

For each of the 39 observed domains, the lattice geometry of the O<sub>2</sub> monolayer and the rotation angle  $\theta$  were analyzed. Domains were identified in the range of  $|\theta| < 6^\circ$ . This is in good agreement with the misalignment with the substrate noted in the previous LEED, i.e., the difference in the spread of the inner spot and the Ag substrate spot,  $\pm 4.7^\circ$  [4]. The lengths of the perpendicular  $h$  and the base  $a$  are plotted as a function of  $\theta$  in Figs. 3(a) and 3(b), respectively. Reflecting the symmetry of the substrate, they are symmetric at positive

TABLE I. The rotation angle between the O<sub>2</sub> monolayer and Ag substrate and the shape of the lattice of the O<sub>2</sub> monolayer. MC: Monte Carlo.

	$\theta$ / deg	$a$ / Å	$\omega_1$ / deg	$\omega_2$ / deg	$(\omega_1 + \omega_2)/2$ / deg	$ \omega_1 - \omega_2 $ / deg	$h$ / Å
Fig. 1(a) upper part	$-1.72 \pm 0.07$	$3.056 \pm 0.006$	$66.2 \pm 0.2$	$71.9 \pm 0.3$	$69.1 \pm 0.2$	$5.7 \pm 0.4$	$3.978 \pm 0.001$
Fig. 1(a) lower part	$+3.15 \pm 0.08$	$3.180 \pm 0.003$	$70.2 \pm 0.1$	$66.3 \pm 0.1$	$68.23 \pm 0.08$	$3.9 \pm 0.2$	$3.987 \pm 0.002$
Fig. 2(a)	$+0.4 \pm 0.1$	$3.22 \pm 0.01$	$67.9 \pm 0.4$	$67.8 \pm 0.3$	$67.8 \pm 0.3$	$0.1 \pm 0.5$	$3.950 \pm 0.002$
Fig. 2(c)	$+3.3 \pm 0.2$	$3.208 \pm 0.006$	$69.5 \pm 0.3$	$66.9 \pm 0.3$	$68.2 \pm 0.2$	$2.6 \pm 0.4$	$3.997 \pm 0.003$
Fig. 2(e)	$-4.1 \pm 0.3$	$3.29 \pm 0.01$	$66.5 \pm 0.4$	$68.6 \pm 0.4$	$67.5 \pm 0.3$	$2.1 \pm 0.6$	$3.968 \pm 0.006$
Total average	$0.5 \pm 2.7$	$3.2 \pm 0.1$			$68.0 \pm 0.7$	$3 \pm 2$	$3.97 \pm 0.03$
Average around $\theta \sim 0^\circ$	$-0.1 \pm 0.4$	$3.23 \pm 0.02$			$67.8 \pm 0.2$	$0.9 \pm 0.7$	$3.96 \pm 0.01$
STM [5]		3.13	71.0	66.2	68.6	4.8	3.98
LEED [4]		3.2			67.8		4.0
MC calculation [9] with spin		3.23	68.3	68.1	68.2	0.2	4.05
MC calculation [9] without spin		3.39	67.1	67.1	67.1	0	4.01

and negative rotation angles  $\theta$ . The length of the perpendicular  $h$  corresponds to the inner spot of the LEED [4] and is in good agreement with the value obtained in the previous study (see Table I). The relationship between the density ( $\rho = 1/ah$ ) of O<sub>2</sub> and the rotation angle  $\theta$  is shown in Fig. 3(c).

There is no domain near  $|\theta| = 1^\circ$ . The reason will be explained later. The gap divides the group into two groups, one near  $\theta = 0$  and the other with  $|\theta| > 1.4^\circ$ . In the group with  $|\theta| > 1.4^\circ$ , the length of the base  $a$  is strongly dependent on the rotation angle  $\theta$ , clearly indicating the influence of the interaction with the Ag substrate. The density  $\rho$  changes from domain to domain due to the stretching and shrinking of the length of the base  $a$ . This suggests that the system shows a rotational epitaxy where the rotation angle to the substrate depends on the density [23]. Such rotational epitaxy had been reported in LEED measurements of O<sub>2</sub> monolayers on graphite [8,10]. In the previous study [10], the rotation angle between the monolayer and the substrate varied with the density that was changed by the amount of adsorption and temperature. Our real-space observation on the Ag surface revealed that domains of different densities were mixed on the same surface. The monolayer might not reach a state of thermal equilibrium within the condition of the present sample preparation. We observed multidomains even after 3 hours annealing at 20 K. To obtain the most stable single domain, prolonged annealing at sufficiently low temperatures so that O<sub>2</sub> do not desorb seems to be necessary.

We found that  $|\theta| > 1.4^\circ$  groups are in a situation of on-line coincidence that has been found in systems of organic molecules [24–27]. Plotting the lattice points of the O<sub>2</sub> obtained in Figs. 2(c) and 2(d) in the unit cell of Ag to which they belong, we obtain Fig. 2(g). Every O<sub>2</sub> lattice point is located on the diagonal of the Ag unit cell.  $s_1 + s_2 \parallel 2a_1 + a_2$  holds, where the basic unit lattice vectors  $s_1$  and  $s_2$  of Ag and  $a_1$  and  $a_2$  of O<sub>2</sub> are defined in Fig. 1(d). As shown in Fig. 2(h), a similar pattern appears for the lattice obtained in Figs. 2(e) and 2(f). Although the rotation angle  $\theta$  is different, the O<sub>2</sub> are aligned on the diagonal of the unit cell as in Fig. 2(g). The results mean that there is one direction in which the reciprocal lattice vector of Ag and that of the O<sub>2</sub> monolayer coincide. We obtain the relation  $s_1^* - s_2^* = a_1^* - 2a_2^*$  at  $\theta > 0$ , and the relation  $s_1^* + 2s_2^* = a_1^* + 3a_2^*$  at  $\theta < 0$ . Here, the primitive vectors of the reciprocal lattice vectors of the substrate are  $s_1^*$  and  $s_2^*$ ,

and those of the O<sub>2</sub> monolayer are  $a_1^*$  and  $a_2^*$ . This situation where the lattice planes of the monolayer and the substrate coincide in only one direction is called on-line coincidence. Historically, the present rotational epitaxy is classified as the line-on-line coincidence [24]. Similar on-line coincidence is also realized in all domains with  $|\theta| > 1.4^\circ$ . For a given local density  $\rho$ ,  $\theta$  is determined to satisfy the on-line coincidence.

The on-line coincidence naturally explains the dependence of the length of the base  $a$  on the rotation angle  $\theta$  shown in Fig. 3(b). When the O<sub>2</sub> are located on the diagonal of the unit cell of Ag, the equation relating the length of the base  $a$  to the rotation angle  $\theta$  can be obtained geometrically as  $a = d \sin 30^\circ / \sin(30^\circ - |\theta|)$ . In Fig. 3(b), the equation of the relationship is depicted as a curve. The agreement between the experiment and the prediction curve is quite good.

Next, we discuss the domains near  $\theta = 0$ . For the domains in Figs. 2(a) and 2(b), the projection of the lattice points of the O<sub>2</sub> onto the Ag unit cell does not reveal any characteristic pattern, and they fill the interior of the Ag unit cell evenly. The domains near  $\theta = 0$  are incommensurate without any coincidence with the substrate. Near  $\theta = 0$ , the effect of interaction with the substrate is considered to be relatively weak. The intrinsic properties of O<sub>2</sub> monolayers that aggregate due to intermolecular forces can be investigated. Averaged over the group near  $\theta = 0$ , the value  $a = 3.23 \pm 0.02$  Å is close to the equilibrium distance of the O<sub>2</sub> – O<sub>2</sub> dimer with H-type configuration (3.2 Å), which was calculated by van der Waals density functional combined with spin-polarization gradient correction [28]. In such an H-type configuration, the O<sub>2</sub> are spin antiparallel, and exchange interactions have also been found to contribute considerably to the stabilization [28]. The intermolecular distance in the O<sub>2</sub> monolayer on an ideally flat substrate was also calculated to be 3.23 Å, which is shorter than the value of 3.39 Å without taking into account the contribution of exchange interactions [9]. We conclude that the system is considered to be antiferromagnetically ordered in the direction where the O<sub>2</sub> are densely aligned with the molecular axes almost parallel to each other. Indeed, previous magnetic susceptibility experiments have suggested short-range antiferromagnetic magnetic ordering in low-density phases on graphite [7].

Here we can discuss the uniaxial distortion of the domain with  $|\theta| > 1.4^\circ$ . When the value of  $a$  obtained near  $\theta = 0$

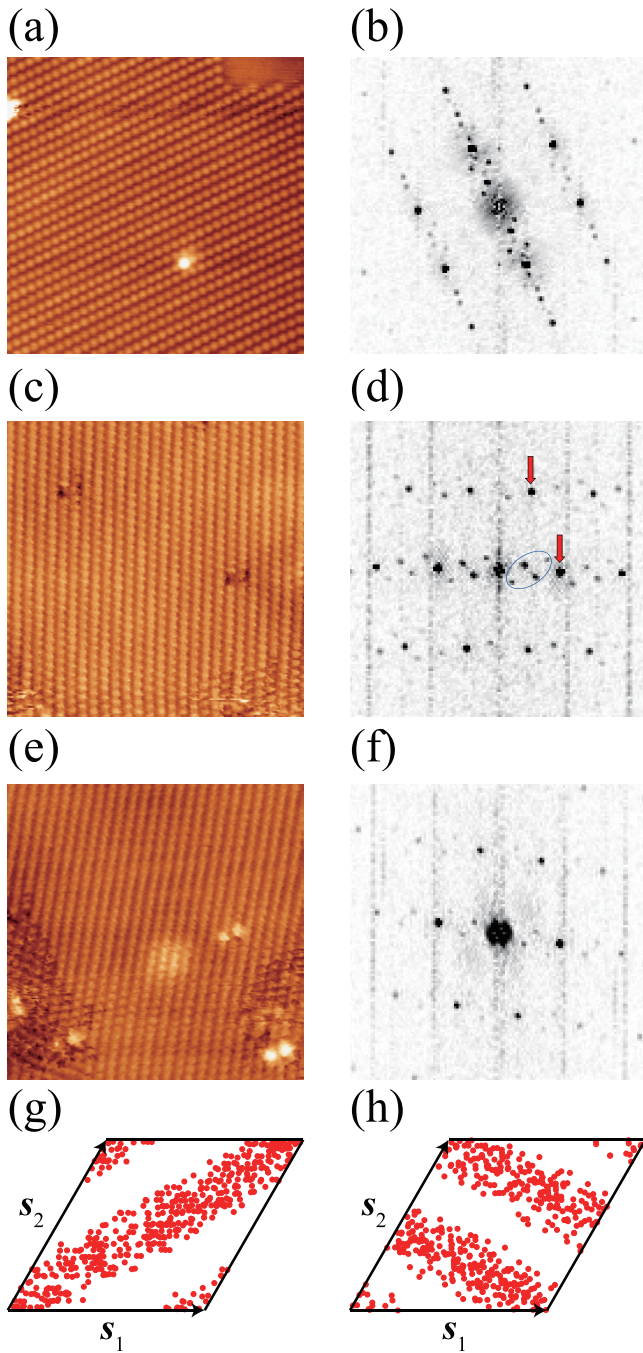


FIG. 2. (a), (c), (e) STM images of  $\text{O}_2$  monolayers: (a)  $10 \times 10 \text{ nm}^2$ ,  $V = 100 \text{ mV}$ ,  $I = 3 \text{ pA}$ ,  $B = 0 \text{ T}$ , (c)  $10 \times 10 \text{ nm}^2$ ,  $V = 50 \text{ mV}$ ,  $I = 3 \text{ pA}$ ,  $B = 11 \text{ T}$ , (e)  $10 \times 10 \text{ nm}^2$ ,  $V = 50 \text{ mV}$ ,  $I = 3 \text{ pA}$ ,  $B = 11 \text{ T}$ . (b), (d), (f) FFT images corresponding to (a), (c), (e):  $5 \times 5 \text{ nm}^{-2}$ . (g), (h) The map of lattice points of  $\text{O}_2$  projected onto a single Ag unit cell corresponding to (c), (e). We randomly selected 500 lattice points of Ag and plotted  $\text{O}_2$  lattice points using the matrix converting the lattice of Ag to the lattice of  $\text{O}_2$  [26].

is regarded as the intrinsic distance between  $\text{O}_2$ , the natural length is also found around  $\theta = 3^\circ$ . For  $|\theta| < 3^\circ$ , it is denser and compressed by up to 6%, and for  $|\theta| > 3^\circ$ , it is less dense and elongated by up to 9%. We cannot find domains near

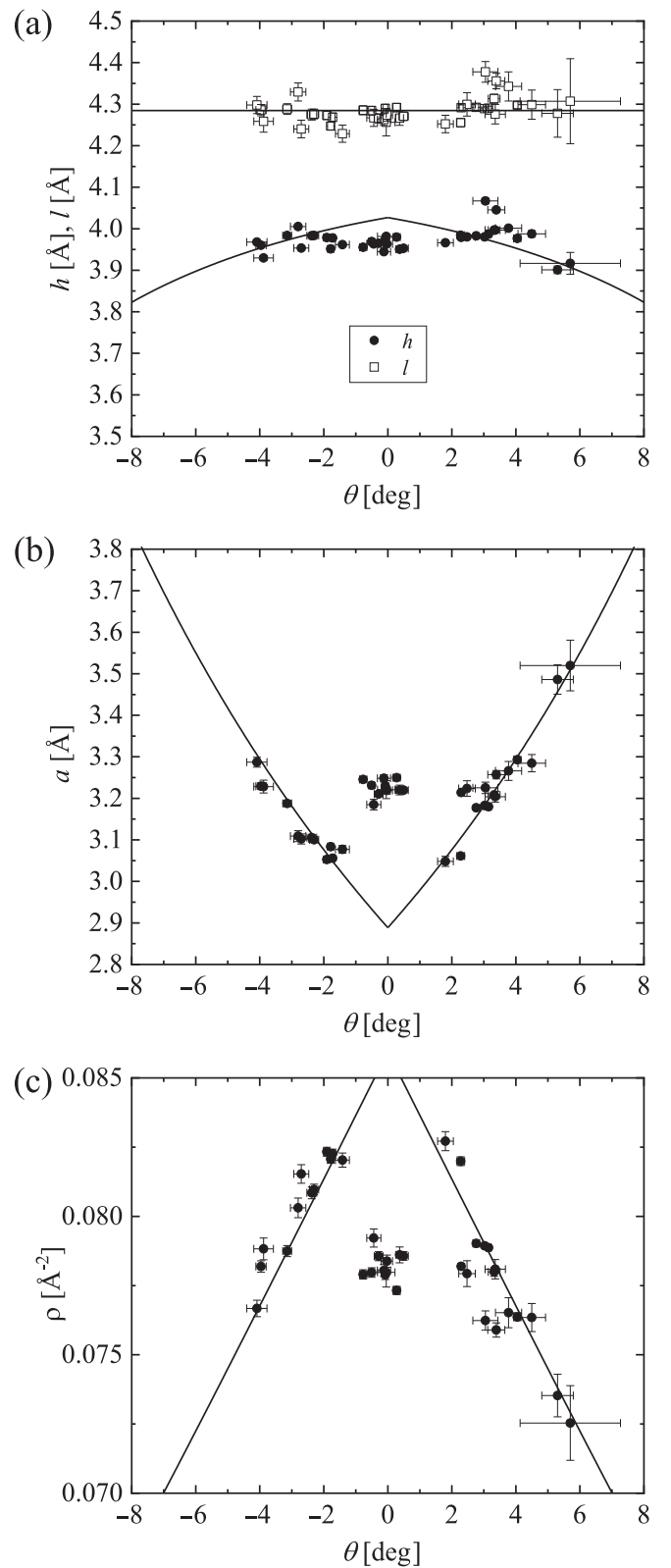


FIG. 3. (a) The average length of the two long sides  $l$  and the length of the perpendicular  $h$  of the  $\text{O}_2$  triangle lattice as a function of  $\theta$ . (b) The length of the base  $a$  of the  $\text{O}_2$  triangle lattice as a function of  $\theta$ . (c) The density  $\rho$  as a function of  $\theta$ . The horizontal line of  $l = 4.28 \text{ \AA}$  and theoretical curves for  $h$ ,  $a$ , and  $\rho$  with  $|\theta| > 1.4^\circ$  are shown.

$|\theta| = 1^\circ$  since the lattice is so compressed that the lattice shape cannot be maintained under the condition of on-line coincidence. On the other hand, the values of  $\theta$  near 0 are selected for the domains without any coincidence with the substrate due to the rotational epitaxy. For the observed domains that deviate from  $\theta = 3^\circ$ , the interaction with the substrate compensates for the loss of intermolecular interaction due to its deformation. According to the intermolecular potential calculation [28], the observed lattice distortion of 9% results in a loss of about 10 meV of energy per molecule. This loss is compensated by the interaction with the Ag substrate. Thus, for the group with  $|\theta| > 1.4^\circ$ , the stabilization energy due to the interaction with the substrate is estimated to be about 10 meV per molecule, on average. According to a previous study, the variation of the adsorption energy of a single O<sub>2</sub> on an Ag(111) substrate depending on the adsorption site is of the order of 100 meV [29]. For the domain of  $|\theta| > 1.4^\circ$ , we find it difficult to study the effect of exchange interaction on the lattice distortion due to the large interaction with the substrate.

## VI. LATTICE DISTORTION

We have discussed the relationship between the density  $\rho$  of the O<sub>2</sub> and the rotation angle  $\theta$  with the substrate, as well as the uniaxial strain due to the interaction with the substrate. We will now discuss one more degree of freedom, shear deformation of the lattice, which has been discussed as the distortion of the lattice due to spin. The two bottom angles  $\omega_1$  and  $\omega_2$  are plotted against the rotation angle  $\theta$  in Fig. 4(a). For the domain with  $|\theta| > 1.4^\circ$ , the bottom angles clearly depend on the rotation angle  $\theta$ .

The shear deformation at  $|\theta| > 1.4^\circ$  is found to be incidental to the on-line coincidence. As shown in Fig. 3(a), the average length of the two long sides,  $l = h(1/\sin \omega_1 + 1/\sin \omega_2)/2$ , is almost independent of the rotation angle  $\theta$ . This implies that O<sub>2</sub> find stable positions on the diagonal of the Ag lattice so that the intermolecular interactions are optimized. Under the condition of on-line coincidence, the bottom angles  $\omega_1$ ,  $\omega_2$  and perpendicular line  $h$  can be determined for given  $l$ . The resulting curves obtained under  $l = 4.28 \text{ \AA}$  are shown in Figs. 4(a) and 3(a). The curves of the simulation explain the observed trend well. It is clear that the lattice distortion in  $|\theta| > 1.4^\circ$  is not caused by exchange interactions in the O<sub>2</sub> monolayer, but is caused by the interaction from the Ag substrate.

Next, we consider the distortion for the domain near  $\theta = 0$ . For a detailed analysis,  $\omega_1 - \omega_2$ , which reflects the magnitude of shear deformation, is plotted against the rotation angle  $\theta$  in Fig. 4(b). On average, we obtain  $|\omega_1 - \omega_2| = 0.9 \pm 0.7^\circ$ . If the distortion from the isosceles triangle is caused by spin, the inequivalence of the two long sides is the origin of the distortion. In the low-density phase, the distance of the long sides is longer than that of the base, so the spin-induced distortion is expected to be small. In addition, the two O<sub>2</sub> in the long side direction have an S-type orientation [see Fig. 1(c)]. The dependence of the pair potential of O<sub>2</sub> - O<sub>2</sub> on molecular orientation has been investigated by previous calculations [28]. In the S-type orientation, the calculated long side lengths are in good agreement with our experiments.

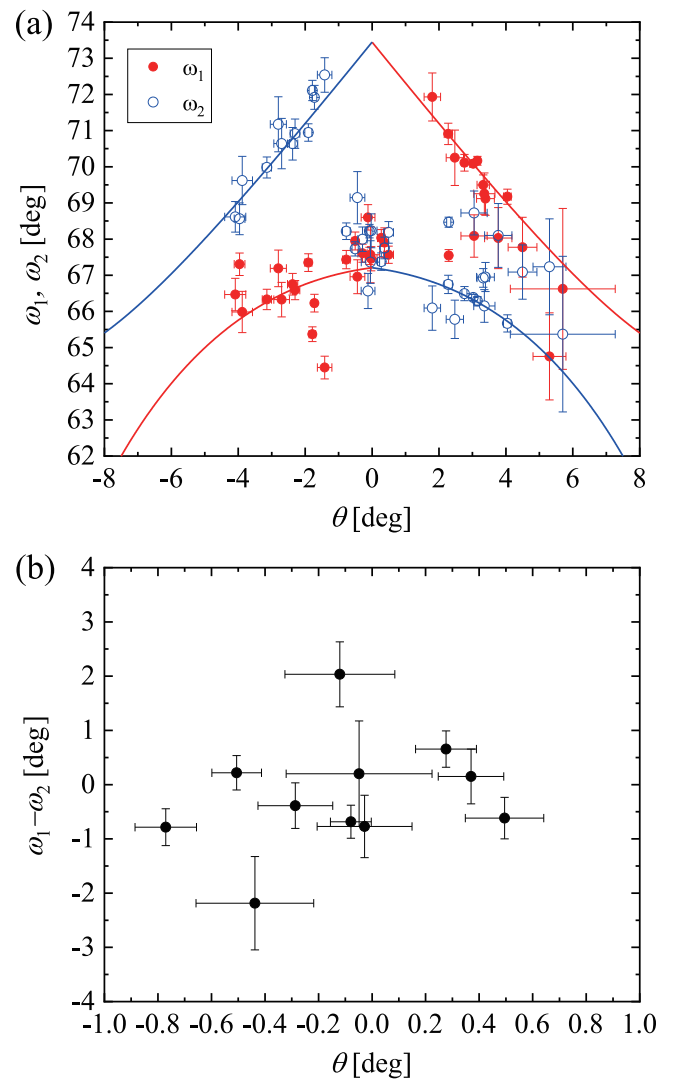


FIG. 4. (a) The base angles  $\omega_1$  and  $\omega_2$  of the O<sub>2</sub> triangle lattice as a function of  $\theta$ . Theoretical curves at  $|\theta| > 1.4^\circ$  are shown. (b)  $\omega_1 - \omega_2$  as a function of  $\theta$  for the domains near  $\theta = 0$ .

According to this calculation, although the S-type orientation also shows antiferromagnetic, the exchange interaction at the long side is of the order of a few meV, which is an order of magnitude smaller than the value at the base. This suggests that the lattice distortion due to magnetic ordering is small in the arrangement of O<sub>2</sub> in the low-density phase. Monte Carlo calculations on a model of the low-density phase on an ideally flat substrate also reported a small value of  $|\omega_1 - \omega_2| = 0.2^\circ$  for the magnetic distortion [9]. We conclude that the exchange interaction makes a detectable contribution to the length of the base  $a$ , but that it makes little contribution to the distortion  $\omega_1 - \omega_2$ . There are only two plots with  $|\omega_1 - \omega_2| > 2^\circ$  in Fig. 4(b). We believe that these are exceptional data points affected by domain boundaries or substrate steps.

In a previous study by STM [5], the distortion was estimated to average  $|\omega_1 - \omega_2| = 4.8^\circ$  across the three domains. Anisotropic exchange interactions were considered to explain this large distortion. The reason why  $\omega_1 - \omega_2$  was estimated to be large in the previous study may be that the domains around

$\theta = 0$  and  $|\theta| = 2^\circ$  were averaged out. In fact, the average value of the length of the base  $a$  of the previous study was estimated to be  $3.13 \text{ \AA}$  smaller than ours, which supports the inclusion of the domain near  $|\theta| = 2^\circ$ , which has a shorter base.

## VII. SUMMARY

In summary, the low-density phases of a monolayer created by adsorbing  $\text{O}_2$  on Ag(111) were observed by high-resolution AFM/STM. Moiré patterns were observed, and the shape of the lattice and the rotation angle between the monolayer and the substrate could be determined with high accuracy. We found that the groups with larger rotation angles show the lattice distortion caused by the interaction with the substrate. On-line coincidence, which had previously been reported only for organic thin films, was found to be possible even for small molecules such as  $\text{O}_2$ . On the other hand, the group with a rotation angle near zero was incommensurate

without any coincidences, and the influence from the substrate could be considered negligible. In this group, lattice distortion could not be confirmed within the measurement error. However, in the direction where  $\text{O}_2$  is densely aligned, antiferromagnetic magnetic ordering is expected to exist. In such a case, it may be a 1D spin chain, so it will be interesting to study its magnetism in the future. On the other hand, as for the observation of lattice distortion due to spin ordering, it is desirable to study the high-density phase [4,7], which forms a nearly equilateral triangular lattice with the densest packing.

## ACKNOWLEDGMENTS

We wish to thank T. Ozaki, M. Fukuda, and Y. Kunisada for fruitful discussions. We acknowledge the support by the JST FOREST Program Grant No. JPMJFR203J and JSPS KAKENHI Grants No. JP20H05178, No. JP20H05849, No. JP21K18867, No. JP22H05448, and No. JP22H01950. Y.S. acknowledges the support of the Asahi Glass Foundation.

- 
- [1] Y. A. Freiman and H. J. Jodl, *Phys. Rep.* **401**, 1 (2004).  
 [2] I. N. Goncharenko, O. L. Makarova, and L. Ulivi, *Phys. Rev. Lett.* **93**, 055502 (2004).  
 [3] M. Hagiwara, M. Ikeda, T. Kida, K. Matsuda, S. Tadera, H. Kyakuno, K. Yanagi, Y. Maniwa, and K. Okunishi, *J. Phys. Soc. Jpn.* **83**, 113706 (2014).  
 [4] Y. Kazama, M. Matsumoto, T. Sugimoto, T. Okano, and K. Fukutani, *Phys. Rev. B* **84**, 064128 (2011).  
 [5] S. Yamamoto, Y. Yoshida, H. Imada, Y. Kim, and Y. Hasegawa, *Phys. Rev. B* **93**, 081408(R) (2016).  
 [6] K. Flurichick and R. D. Eppers, *J. Chem. Phys.* **84**, 4657 (1986).  
 [7] Y. Murakami, *J. Phys. Chem. Solids* **59**, 467 (1998).  
 [8] M. F. Toney, R. D. Diehl, and S. C. Fain, *Phys. Rev. B* **27**, 6413 (1983).  
 [9] R. D. Eppers and O. B. M. Hardouin Duparc, *Phys. Rev. B* **32**, 7600 (1985).  
 [10] M. F. Toney and S. C. Fain, *Phys. Rev. B* **36**, 1248 (1987).  
 [11] F. Haldane, *Phys. Lett. A* **93**, 464 (1983).  
 [12] K. Niki, S. Ogura, M. Matsumoto, T. Okano, and K. Fukutani, *Phys. Rev. B* **79**, 085408 (2009).  
 [13] Y. Kunisada, H. Nakanishi, W. A. Dio, and H. Kasai, *Current Appl. Phys.* **12**, S115 (2012).  
 [14] Y. Sugimoto and J. Onoda, *Appl. Phys. Lett.* **115**, 173104 (2019).  
 [15] See Supplemental Material at <http://link.aps.org/supplemental/10.1103/PhysRevB.106.115432> for the magnetic field dependence of the results.  
 [16] D. Neas and P. Klapetek, *Cent. Eur. J. Phys.* **10**, 181 (2012).  
 [17] K. Momma and F. Izumi, *J. Appl. Crystallogr.* **44**, 1272 (2011).  
 [18] L. Gross, F. Mohn, N. Moll, P. Liljeroth, and G. Meyer, *Science* **325**, 1110 (2009).  
 [19] A. Shiotari, N. Takahiro, I. Kota, M. Shigeeki, O. Tetsuo, S. Hiroshi, and Y. Sugimoto, *Nat. Commun.* **8**, 16089 (2017).  
 [20] A. Shiotari and Y. Sugimoto, *Nat. Commun.* **8**, 14313 (2017).  
 [21] R. Ma, D. Cao, C. Zhu, Y. Tian, J. Peng, J. Guo, J. Chen, X.-Z. Li, J. S. Francisco, X. C. Zeng, L.-M. Xu, E.-G. Wang, and Y. Jiang, *Nature (London)* **577**, 60 (2020).  
 [22] S. Günther, P. Zeller, B. Blller, and J. Wintterlin, *ChemPhysChem* **22**, 870 (2021).  
 [23] A. D. Novaco and J. P. McTague, *Phys. Rev. Lett.* **38**, 1286 (1977).  
 [24] S. C. B. Mannsfeld, K. Leo, and T. Fritz, *Phys. Rev. Lett.* **94**, 056104 (2005).  
 [25] C. Wagner, R. Forker, and T. Fritz, *J. Phys. Chem. Lett.* **3**, 419 (2012).  
 [26] R. Forker, M. Meissner, and T. Fritz, *Soft Matter* **13**, 1748 (2017).  
 [27] F. Bocquet, L. Nony, S. C. B. Mannsfeld, V. Oison, R. Pawlak, L. Porte, and C. Loppacher, *Phys. Rev. Lett.* **108**, 206103 (2012).  
 [28] M. Obata, I. Hamada, and T. Oda, *JPS Conf. Proc.* **5**, 011011 (2015).  
 [29] Y. Kunisada, H. Nakanishi, and H. Kasai, *J. Phys. Soc. Jpn.* **80**, 084605 (2011).